Marine Pollution Bulletin 164 (2021) 112076

Contents lists available at ScienceDirect

Marine Pollution Bulletin

journal homepage: www.elsevier.com/locate/marpolbul

Mapping spatial and temporal variation of seafloor organic matter $\Delta^{14}C$ and $\delta^{13}C$ in the Northern Gulf of Mexico following the Deepwater Horizon Oil Spill

Kelsey L. Rogers [a,*], Samantha H. Bosman [a], Natalie Wildermann [a], Brad E. Rosenheim [b], Joseph P. Montoya [c], David Hollander [b], Tingting Zhao [d], Jeffrey P. Chanton [a,**]

[a] Department of Earth, Ocean and Atmospheric Science, Florida State University, 1011 Academic Way, Tallahassee, FL 32306-4350, United States
[b] College of Marine Science, University of South Florida, 140 7th Avenue South, St. Petersburg, FL 33701, United States
[c] School of Biological Sciences, Georgia Institute of Technology, 310 Ferst Dr NW, Atlanta, GA 30332, United States
[d] Department of Geography, Florida State University, 113 Collegiate Loop, Tallahassee, FL 32306-2190, United States

ARTICLE INFO

Keywords:
Deepwater Horizon
Radiocarbon
Sediments
Gulf of Mexico
Carbon isotopes
Petrocarbon

ABSTRACT

Following the Deepwater Horizon oil spill of 2010, large amounts of biodegraded oil (petrocarbon) sank to the seafloor. Our objectives were to 1) determine post-spill isotopic values as the sediments approached a new baseline and 2) track the recovery of affected sediments. Sediment organic carbon $\delta^{13}C$ and $\Delta^{14}C$ reached a post-spill baseline averaging $-21.2 \pm 0.9‰$ ($n = 129$) and $-220 \pm 66‰$ ($n = 95$). Spatial variations in seafloor organic carbon baseline isotopic values, ^{13}C and ^{14}C, were influenced by river discharge and hydrocarbon seepage, respectively. Inverse Distance Weighting of surface sediment $\Delta^{14}C$ values away from seep sites showed a 50% decrease in the total mass of petrocarbon, from 2010 to 2014. We estimated a rate of loss of -2×10^9 g of petrocarbon-C/year, 2–11% of the degradation rates in surface slicks. Despite the observed recovery in sediments, lingering residual material in the surface sediments was evident seven years following the blowout.

1. Introduction

The term "petrocarbon" has been used to describe crude oil or transformed crude oil following biodegradation, weathering, oxygenation or loss of lighter components. The category includes methane or oil derived carbon assimilated or incorporated into microbial biomass (Cherrier et al., 2014) or into the food web (Chanton et al., 2012; Wilson et al., 2016). Petrocarbon is distinct from "petrogenic" carbon which includes petroleum-derived fossil (aged, radiocarbon (^{14}C) depleted) carbon but also fossil carbon released from rocks. Carbon isotopes (^{13}C, ^{14}C) can be used to determine a molecule's source and can reveal the presence of petrocarbon even when the original hydrocarbons have been biodegraded or otherwise transformed and have lost their unique chemical structures. For example, a petroleum-based compound can be oxygenated, altering the molecule's polarity, solubility, and reactivity, yet the molecule will still carry the original ^{13}C and ^{14}C isotopic signature (Sun et al., 2005; Aeppli et al., 2012; Ruddy et al., 2014). Many studies have used carbon isotopes to study the presence and degradation of hydrocarbons in the environment including: Zafiriou (1973), White et al. (2008) and Bostic et al. (2018).

Petrocarbon from the Deepwater Horizon (DWH) blowout was transported to the seafloor and originated from degraded products derived from at least two major sources: 1) surface slicks and 2) the deep-water hydrocarbon plume. Surface slicks led to the formation of marine oil-derived material snow (MOS). The degraded floating oil-derived material interacted with other floating particles, phytoplankton, and exopolymeric substances from oil-degrading bacteria to form aggregates that were large enough to sink quickly without the hydrocarbon-derived material degrading completely to CO_2 before deposition (Passow et al., 2012). Yan et al. (2016) found barium from drilling mud and PAHs in marine snow for five months following the capping of the well. Chanton et al. (2018) found evidence that petrocarbon persisted for as long as three years in sinking particulate organic carbon after the spill. Rogers et al. (2019b) found that suspended POC in deep waters retained the isotopic signature of the spilled oil for four years. The Marine Oil Snow Sedimentation and Flocculent

* Corresponding author.
** Corresponding author at: Department of Geosciences and Natural Resources Management, University of Copenhagen, Copenhagen, Denmark.
E-mail addresses: klrogers8@gmail.com (K.L. Rogers), jchanton@fsu.edu (J.P. Chanton).

https://doi.org/10.1016/j.marpolbul.2021.112076
Received 22 April 2020; Received in revised form 14 January 2021; Accepted 18 January 2021
Available online 30 January 2021

Accumulation (MOSSFA; Daly et al., 2016; Burd et al., 2020) event following the DWH blowout, temporarily increased sedimentation rates, rapidly depositing up to 1 cm of degraded petrocarbon-rich material over the course of four to five months (Brooks et al., 2015; Schwing et al., 2017). The deep-water hydrocarbon plume which formed between 1000 and 1200 m (Valentine et al., 2010) carried an estimated 30% of the total mass of material released from the well (Ryerson et al., 2012). It was suggested that most of the sedimented petrocarbon came from this deep-water hydrocarbon plume because of the differences in the coverage area and the composition of material in the surface slicks and the sedimented material (Mason et al., 2014; Valentine et al., 2014). Others saw a more important role for surface material's contribution to the sedimented residue (Passow and Hetland, 2016; Passow and Ziervogel, 2016).

The oil budget calculator group estimated that 11–30% of the discharged oil remained unaccounted for (Lehr et al., 2010), possibly sinking to the seafloor following partial biodegradation. Several studies since have looked at the coverage areas and effects of sedimented oil-residue following the DWH blowout. Independent studies found signs of oil-residue contamination in sediment across the northern Gulf of Mexico (GOM) (Valentine et al., 2014; Chanton et al., 2015). Using radiocarbon (^{14}C) as a tracer of fossil carbon released into the environment (Bosman et al., 2017), it was estimated that 0.5–9.1% of the total oil released sank to the seafloor as petrocarbon, creating areas with depleted radiocarbon signatures in the surface sediment (0–1 cm) (Chanton et al., 2015). This estimate was similar to Valentine et al. (2014) estimate of 1.8–14.4% that was calculated from elevated levels of the biomarker, hopane. Stout et al. (2016) estimated between 6.9 and 7.7% of the total released oil was deposited on the seafloor also analyzing hopane. They also found an 80–90% decrease in the concentration of total hopane and PAH in surface sediments by 2014. However, loss of hopane biomarker compounds does not equate to loss of petrocarbon. Decreases in hopane could be due to degradation of the hopane into oxygenated non-hopane compounds (Aeppli et al., 2012; Aeppli et al., 2018; Ruddy et al., 2014). Tracing petrocarbon with ^{14}C, captures the signal of all unaltered and transformed petrocarbon compounds, allowing the quantification of fresh or degraded petrocarbon and, in addition, petrocarbon incorporated into microbial biomass. Applying both isotopic and specific compound tracing methods provides a more complete picture of the recovery of GOM sediments.

Passow and Ziervogel (2016) suggested that the estimates of oil-residue deposition described above underestimated both the total area that was affected and the amount of oil-residue that was deposited on the seafloor. They argued that sediment coring of the seafloor was focused to the southwest of the wellhead, in a small area, but MOS also formed outside of this area and to the northeast in the Desoto Canyon. Once the MOS was deposited, other processes such as bioturbation, degradation, and resuspension masked or redistributed the material (Diercks et al., 2018). Chemical analysis of 2613 sediment cores taken between 2010 and 2011 from the Gulf of Mexico indicated that oil from the DWH was detectable in sediments up to 517 km from the wellhead, and contaminated an area of ~110,000 km^2 and that 21 ± 10% of the unrecovered oil from the DWH spill may have been deposited on the seafloor (Romero et al., 2017). Once sedimented, rates of petrocarbon degradation were dependent on the level of initial contamination (Bagby et al., 2016). High contamination levels reduced rates of degradation, while low contamination was associated with higher degradation rates (% per day, Bagby et al., 2016).

Whether chemical tracers like hopane or isotopic tracers like radiocarbon are applied, accounting for petrocarbon accumulation in the sediments is dependent on determination of baseline concentrations or signatures. We previously estimated that the background $\Delta^{14}C$ signature below the surface 2 cm of sediment was constant (−200 ± 29‰) for several cm below and over a broad area around the wellhead site due, in part, to the high sedimentation rates of this setting (Chanton et al., 2015; Adhikari et al., 2016). This signature is more depleted than the background value of particles sinking through the water column which had a $\Delta^{14}C = 3.8 \pm 31.1$‰ (Chanton et al., 2018; Giering et al., 2018) and riverine input from the Mississippi River, which averages $\Delta^{14}C = -154 \pm 68$‰ (Cai et al., 2015). The lower background signature of the sediments is due to bioturbation mixing new inputs of sediment with deeper, older underlying sediment and likely due to preferential remineralization of modern carbon, relative to older material, on the seafloor.

The first goal of this study was to determine the post-spill background or baseline $\Delta^{14}C$ and $\delta^{13}C$ in the surficial sediment of the northern GOM. To accomplish this, we characterized the spatial trends of ^{13}C and ^{14}C on the seafloor, excluding the most petrocarbon-impacted samples from 2010, to determine how photosynthetic, riverine, and inputs from natural hydrocarbon seeps contribute to and affect the baseline isotopic composition of the sedimentary organic carbon pool across spatial scales of the northern Gulf. A second goal was to assess the recovery in the northern Gulf's surface sediment affected by the DWH blowout by tracking $\Delta^{14}C$ signatures from 2010 through time in the vicinity of the wellhead. We hypothesized that we would detect decreasing evidence of petrocarbon in the sediments after 2010, which would be observed by an enrichment in ^{14}C isotopic signatures.

2. Materials and methods

2.1. Sample collection and processing

Surface sediment was collected and analyzed for $\delta^{13}C$ and $\Delta^{14}C$ from 199 sites by multicore over seven years, from 2010 to 2017, across the northern GOM (Fig. 1). The surfaces, 0–1 cm, of all cores were collected and frozen until processing in the lab. The sediment was acid treated with 10% HCl, to remove carbonates, rinsed, freeze dried, and ground. Sites were categorized as seep or non-seep according to map data compiled by MacDonald et al. (2015) and shipboard acoustics that detect features like hard bottoms or bubble streams that indicate potential seep sites.

2.2. $\delta^{13}C$ and $\Delta^{14}C$ analysis

Sediment was analyzed for $\delta^{13}C$ and %C using a Carlo-Erba elemental analyzer connected to a Finnigan MAT delta Plus XP Stable Isotope Ratio Mass Spectrometer (EA-IRMS) at the National High Magnetic Field Laboratory. Samples collected after 2016 were sent to the Duke Environmental Stable Isotope Laboratory. For natural abundance of radiocarbon, a subset of samples was combusted in quartz tubes at 850 °C for 4 h and the resultant CO_2 was purified cryogenically using the methods of Choi and Wang (2004). The purified CO_2 was flame sealed in a 6 mm ampoule and sent to Woods Hole National Ocean Sciences Accelerator Mass Spectrometry (NOSAMS) or University of Georgia (UGA) for analysis of natural abundance of radiocarbon. The radiocarbon signatures are reported in $\Delta^{14}C$ notation as described by Stuiver and Polach (1977). The ^{14}C blanks were generally between 1.2 and 5 micrograms of C, producing a negligible effect on samples, which were over 1200 micrograms of C. The analysis of 22 replicate sediment samples yielded an average analytical reproducibility of ±6.8‰ for $\Delta^{14}C$ and 0.2‰ for $\delta^{13}C$. Forty coal samples, representing fossil ^{14}C dead carbon, were analyzed to assess our procedural blank of combustion, graphitization, and target preparation, over the course of this study. The average $\Delta^{14}C$ value was −995 ± 7‰. We also ran 25 azalea leaf standards collected in Tallahassee, Florida in 2013; the average $\Delta^{14}C$ value was 31 ± 8‰. There was no variation between AMS labs in these samples or the coal blanks.

2.3. Calculations for petrocarbon coverage area and percent contribution to surface sediments

To determine spatial trends in the surface sediments, we used the

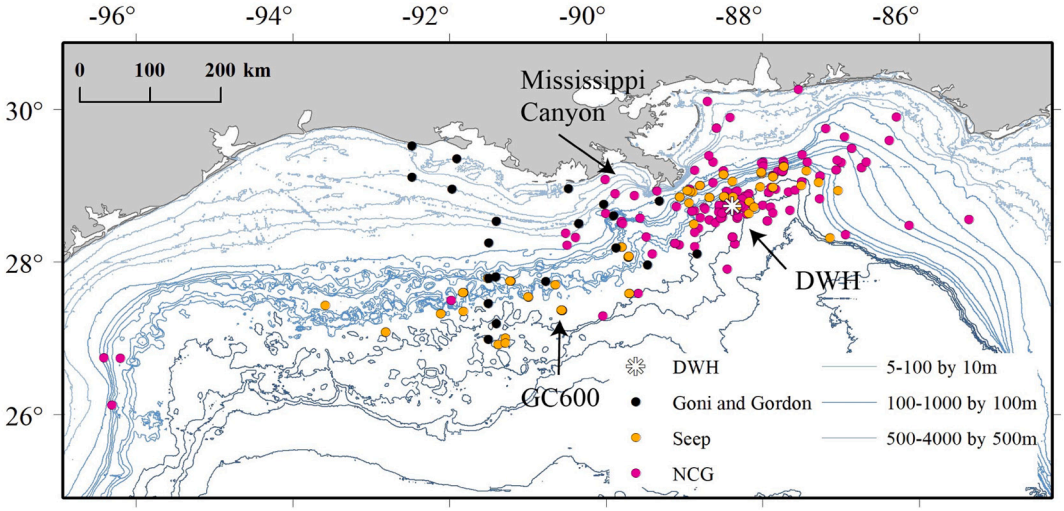

Fig. 1. Map of all surface sediment samples from northern Gulf of Mexico collected from 2010 to 2017, including sediment collected by Goni et al. (1998) and Gordon and Goni (2003) (black). NCG stands for North Central Gulf non-seep sites (pink) and Seep sites in yellow. (For interpretation of the references to color in this figure legend, the reader is referred to the web version of this article.)

Inverse Distance Weighting (IDW) method in ArcGIS 10.2.2 to interpolate the data. IDW predicts the value of an unknown area using the weighted distance to known points. Closer points are weighed more heavily than measurements further away. By varying the search radius (3 to 6 by each integer increment) and power (1–3 by 0.5 increment) terms used in the IDW, we reduced the effect of overpowering the nearest samples on the estimated values of unknown areas (Chanton et al., 2015). This also allows the analysis to be more flexible, reducing the assumption of the spatial autocorrelation of the data. Following the procedure in our earlier paper, Chanton et al. (2015), one of the points from 2010 was buffered to 5 km to limit the effect of the depleted signatures of the sediment from over influencing estimates in the surrounding sediments. To determine temporal trends in the data, the radiocarbon signatures were grouped into 20‰ bins from −40 to −500‰, from which we calculated the area covered by each bin and the petrocarbon incorporated into the surface sediment. We calculated the fraction petrocarbon contributed from each bin $\Delta^{14}C$ value using similar calculations to Chanton et al. (2015):

$$Average\ bin\ ^{14}C\ value^{*}1 = x(-1000‰) + (1-x)(-200‰)$$

with the background of $\Delta^{14}C = -200‰$ (Chanton et al., 2015). The result was multiplied by the average percent organic carbon of the sediment (1.8 ± 0.7%) and the bulk density (0.21 ± 0.04 g/cm^3). We integrated this value to 1 cm and multiplied it by the areas from each IDW interpolation to calculate the grams of carbon from petrocarbon within the polygon. Uncertainties were calculated by varying the organic carbon percent and bulk density according to the uncertainties listed above. Sediment with $\Delta^{14}C$ signatures greater than −200‰ were considered free of petrocarbon. The bulk density was measured in a subset of petrocarbon affected cores and has been used in other studies to convert from volume to grams of contaminated sediments (Valentine et al., 2014; Romero et al., 2017).

3. Results and discussion

3.1. Mapping isotopic values of surface sediments

Surface sediment from all sampling years, including both seep and North Central Gulf (NCG; non-seep) sites, had $\delta^{13}C$ signatures ranging from −44.5‰ to −16.0‰, averaging −22.6 ± 3.4‰ ($n = 326$) and $\Delta^{14}C$ signatures ranging from −910‰ to −23‰ averaging −280 ± 167‰ ($n = 211$). Surface sediment from NCG (non-seep) stations only (including 2010, excluding seep) had $\delta^{13}C$ signatures ranging from −23.7‰ to −16.0‰, averaging −21.3 ± 0.9‰ ($n = 207$), and $\Delta^{14}C$ signatures ranging from −501‰ to −23‰, averaging −221 ± 79‰ ($n = 135$). Excluding 2010, the most impacted year, NCG surface sediment had $\delta^{13}C$ ranging from −22.8‰ to −16.0, averaging −21.2 ± 0.9‰ ($n = 129$), and $\Delta^{14}C$ ranging from −468‰ to −58‰ averaging −220 ± 66‰ ($n = 95$). Data are presented in Supplementary Table 1 and archived at https://data.gulfresearchinitiative.org, DOI https://doi.org/10.7266/N7Q52N7D.

Our first objective was to determine the overall isotopic spatial trends in the surface sediment of the northern GOM. We created four sediment surface maps of $\delta^{13}C$ and $\Delta^{14}C$, with one set using North Central Gulf (NCG, non-seep) sediment and including data collected by Goni et al. (1998) and Gordon and Goni (2003) (Fig. 2) and a second set using this same data and also sediments collected at seep sites (Fig. 3). In these spatial maps and analyses (Figs. 2 and 3), we did not include surface sediment from 2010, which was most affected by the oil spill (Rogers et al., 2019a), as our goal was to determine the system's baseline/background values. We treated the data in two categories, non-seep and seep, after finding significant differences between the $\delta^{13}C$ and $\Delta^{14}C$ signatures of non-seep and seep sediment using the Mann-Whitney *U* test ($\delta^{13}C$: U = 1179, $p < 0.0001$, non-seep median = −21.2‰, seep median = −23.6‰; $\Delta^{14}C$: U = 1934, $p < 0.0001$, non-seep median = −214‰, seep median = −327‰). Different color scales were used in Figs. 2 and 3 to better visualize differences in the isotopic signatures from non-seep sites only (Fig. 2). The overall variation caused by seep areas would overpower variability at the NCG sites. There is a possibility that some sediment was taken from more ephemeral seep areas, which may not release hydrocarbons regularly and which were not mapped in MacDonald et al. (2015). However, given that our median $\Delta^{14}C$ signature is within our background range, we do not think we misclassified many sites.

3.2. Spatial trends in isotopic composition in North Central Gulf surface sediments (non-seep)

We observed an east-west longitudinal trend in the $\delta^{13}C$ of surface sediment of non-seep sites, with more enriched $\delta^{13}C$ signatures towards the Florida shelf, becoming significantly more depleted towards the west (Figs. 2A, 4A, $p < 0.0001$). The three samples collected west of 96W (points 323–325, Supplementary Fig. 1), were not included in the regression analyses that follow because of their distance away from the

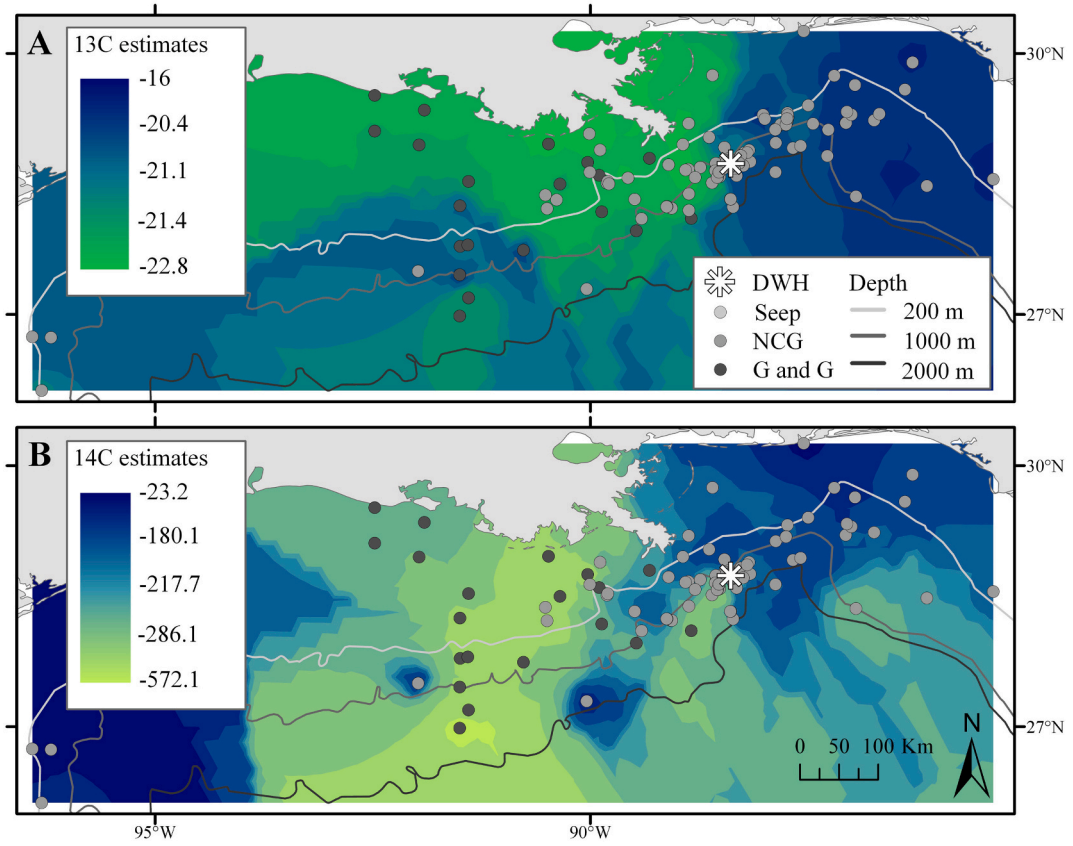

Fig. 2. Averaged inverse distance weighing (IDW) interpolations of A) $\delta^{13}C$ and B) $\Delta^{14}C$ of Northern Central Gulf (NCG, non-seep) sediment (gray circles) sampled from 2011 to 2017 including sediment reported by Goni et al. (1998) and Gordon and Goni (2003) (G and G, dark gray circles). A white star marks the site of the Deepwater Horizon wellhead.

location of most data. In this treatment, most depletion in $\delta^{13}C$ was observed near the mouth of the Mississippi River and along the coastline of Louisiana, due to the influence of terrestrial/riverine inputs. Organic carbon coming from the Mississippi River has a $\Delta^{14}C = -154 \pm 68‰$ and $\delta^{13}C = -26 \pm 1‰$ (Cai et al., 2015). Sorting and differential sedimentation occurs across the nearshore to the offshore, with larger sized terrestrial-derived material dropping out close to shore (Bianchi et al., 2002). The IDW map of ^{14}C suggested a similar east-west trend with more depleted values found in the west, (Fig. 2B), but the relationship of $\Delta^{14}C$ of non-seep sites with longitude was not significant (Fig. 4B, $p = 0.3323$). Again, the western most samples, west of 96W (points 323–325, Supplementary Fig. 1) were not included in this analysis. There was a swath of more ^{14}C depleted sediment south of Louisiana and west of the Mississippi Canyon, running N-S from the coastline at about 91 W (south of site 343, Supplementary Fig. 1), potentially derived from older terrestrial material (Fig. 2B). To the east of this depleted swath, in the vicinity of the Mississippi Canyon (Figs. 1, 2B), there was a strip of more enriched, modern carbon running N-S at about 90W (south of site 156, Supplementary Fig. 1). As organic material is delivered to the GOM by the Mississippi River, sediment is deposited along the continental shelf above this canyon and remobilized, transporting between 40 and 50% of the sediment down slope (Corbett et al., 2004; Corbett et al., 2006). The nutrients and lithogenic material delivered by the Mississippi River are drivers for increased productivity in the surface waters, which could cause enrichment in $\Delta^{14}C$ and potentially increased sedimentation of sinking particles, by flocculation/aggregation (Chanton et al., 2018; De La Rocha and Passow, 2007). There was also a highly depleted hot spot to the south of Louisiana, which was collected by Goni et al. (1998) and Gordon and Goni (2003) and was potentially influenced by the mega seep GC600 (Figs. 1, 2; site 232, Supplementary Fig. 1).

There was a significant relationship between $\delta^{13}C$ of non-seep (NCG) sediment and latitude (Fig. 4C, $p = 0.0018$), probably due to the importance of the Mississippi River and terrestrial organic matter nearshore, and sediments acquiring a more marine $\delta^{13}C$ going offshore, from north to south. The $\delta^{13}C$ of the riverine input is $-26 \pm 1‰$ (Cai et al., 2015), mixing with marine primary production of $\delta^{13}C = -21 \pm 2‰$ (Chanton et al., 2012, 2018). The influence of the Mississippi River is seen just south of the mouth of the river, while more marine influence is seen to the eastern side of the map. There is a significant linear correlation between $\Delta^{14}C$ and latitude at seep sites, which drives the overall correlation between $\Delta^{14}C$ and latitude in the northern GOM. However, we did not find a significant linear correlation between $\Delta^{14}C$ of non-seep sediments and latitude (Fig. 4D, $p = 0.2214$), showing that the Mississippi is important to the $\delta^{13}C$ of nearshore sediments, but apparently does not have such a strong effect on $\Delta^{14}C$ signatures. This is likely due to the lack of difference between the ^{14}C value of Mississippi river particulates and the surface sediments of the northern Gulf. Consideration of the two and three endmember mixing models that have been applied in other studies (Chanton et al., 2012; Cherrier et al., 2014; Rogers et al., 2019b), indicates the similarity between the Mississippi input and GOM background sediment with $\Delta^{14}C$ endmembers of $-154 \pm 68‰$ and $-200 \pm 29‰$, respectively. Additionally, perhaps the delivery of older particulates by the river is offset by increased primary production due to nutrient delivery. We found no significant linear correlation between water depth and $\delta^{13}C$ (Fig. 4E) or $\Delta^{14}C$ (Fig. 4F) for non-seep and seep sediments. Similarly, Rosenheim et al. (2016) observed no relationship between depth and the $\delta^{13}C$ of pre-spill sediments. The equations below refer to Fig. 4 and the panels within.

A) $\delta^{13}C$ vs longitude:

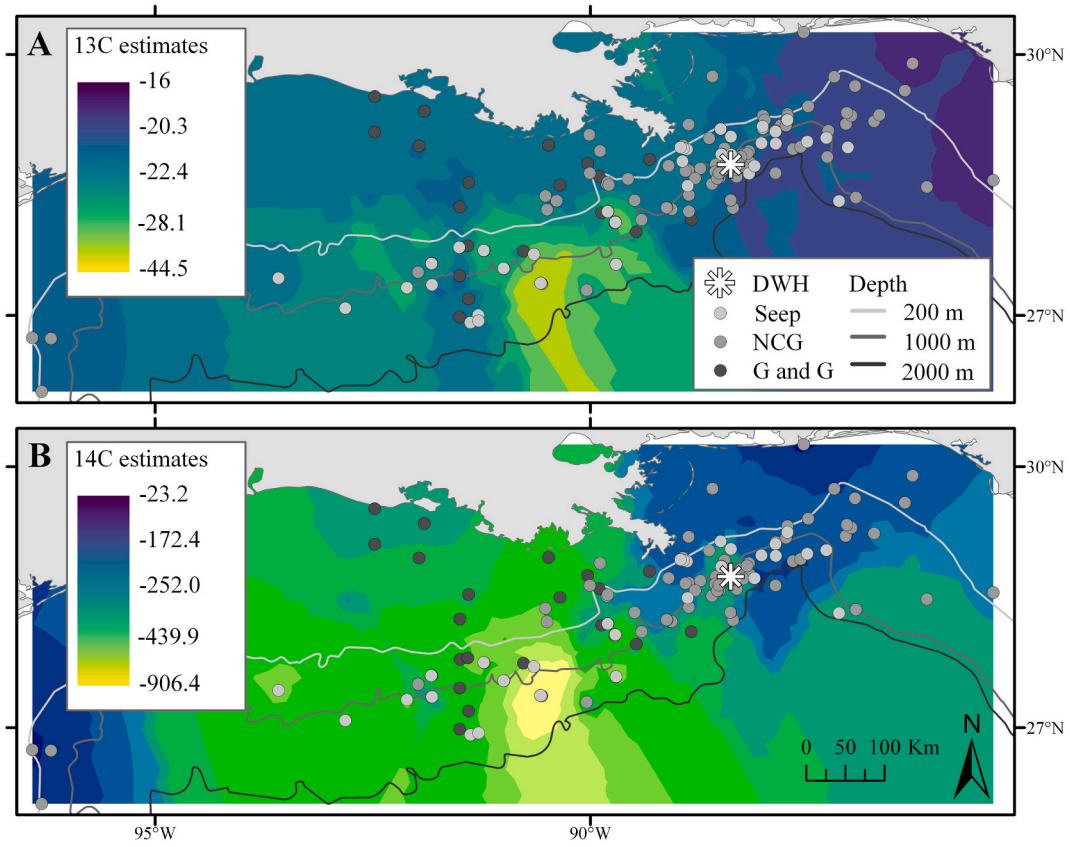

Fig. 3. Average IDW interpolation of A) $\delta^{13}C$ and B) $\Delta^{14}C$ of surface Gulf of Mexico sediment, including Northern Central Gulf (NCG, non-seep) sediment (gray circles), seep sediment (light gray circles), (2011–2017) and sediment reported by Goni et al. (1998) and Gordon and Goni (2003) (G and G, dark gray circles). A white star marks the site of the Deepwater Horizon wellhead.

non-seep: y = 0.5112x + 23.974; $r = 0.5367$; $n = 120$; $p < 0.0001$;
seep: y = 0.6138x + 30.102; $r = 0.1788$; $n = 114$; $p = 0.0559$.
all: y = 1.1656x + 80.82, $r = 0.4370$, $n = 234$, $p < 0.0001$.

B) $\Delta^{14}C$ vs longitude:

non-seep: y = 4.668x + 192.7; r = 0.1, $n = 89$; $p = 0.3484$;
seep: y = 60.61x + 5078; $r = 0.374$; $n = 72$; $p = 0.0011$.
all: y = 56.68x + 4762, $r = 0.4690$, $n = 161$, p < 0.0001.

C) $\delta^{13}C$ vs latitude:

non-seep: y = 0.587x − 38.086; $r = 0.2742$; n = 120; $p = 0.0023$;
seep: y = 2.6828x − 100.33; $r = 0.3638$; n = 114; p < 0.0001.
all: y = 3.0218x − 108.99, $r = 0.5205$, n = 234, p < 0.0001.

D) $\Delta^{14}C$ vs latitude:

non-seep: y = 18.09x − 739.55; $r = 0.128$; n = 89; $p = 0.2292$;
seep: y = 197.37x − 5911; $r = 0.535$; n = 72; p < 0.0001.
all: y = 153.69x − 4667, $r = 0.5629$, n = 161, p < 0.0001.

E) $\delta^{13}C$ vs water depth:

non-seep: $y = 9 \times 10^{-5}x - 21.27$; $r = 0.003$; n = 120; $p = 0.9739$;
seep: y = −0.0016x − 23.831; $r = 0.0193$; n = 114; $p = 0.1388$.
all: y = 0.0003x − 23.42, $r = 0.0019$, n = 234, $p = 0.9768$.

F) $\Delta^{14}C$ vs water depth:

non-seep: y = −0.0172x − 198.36; $r = 0.1513$; n = 89; $p = 0.1546$;
seep: y = −0.1886x − 233.6; $r = 0.2927$; n = 72, $p = 0.012$.
all: y = 0.0011x − 294.43, $r = 0.0031$, n = 161, $p = 0.9688$.

3.3. Spatial trends in surface sediment isotopic composition at all sites including those identified as seep sites

The influence of seep sites has been observed in the water column (D'souza et al., 2016) and we wanted to determine the impact of seepage on surface sediment $\delta^{13}C$ and $\Delta^{14}C$ signatures in the northern GOM. We hypothesized that there would be an east-west longitudinal gradient with more depleted $\delta^{13}C$ and $\Delta^{14}C$ in the west, caused by the increasing importance of natural hydrocarbon seepage. To test this hypothesis, we built on to Fig. 2, adding all surface sediment collected from seep sites (Fig. 3). The east-west trend that was apparent in Fig. 2A-B is also present in Fig. 3A-B; however, this gradient is enhanced due to presence of the seep sites (Fig. 4A, B, p < 0.0001 for all sites for both isotopes versus longitude). For seep sites only, there was no correlation between $\delta^{13}C$ and longitude ($p = 0.063$, Fig. 4), but for ^{14}C, there was a significant correlation (p = 0.0011). These results indicate that river discharge primarily influences our observed ^{13}C distributions while seepage is a more important influence for ^{14}C. Riverine organic carbon has a signature of $\Delta^{14}C = -154 \pm 68‰$ and $\delta^{13}C = -26 \pm 1‰$ (Cai et al., 2015), marine primary production has values of $\Delta^{14}C = 38.8 \pm 25.8‰$, and $\delta^{13}C = -21 \pm 2‰$ (Chanton et al., 2012, 2018). Oil and methane released from the Macondo wellhead is presumably similar to seeps in the area with $\Delta^{14}C = -1000‰$ and $\delta^{13}C$ of oil = −27‰ (Graham et al., 2010) and $\delta^{13}C$ of methane = −57.4‰ (Crespo-Medina et al., 2014). The background $\Delta^{14}C$ signature of GOM sediment is about −200‰. The difference in radiocarbon isotope space between the riverine

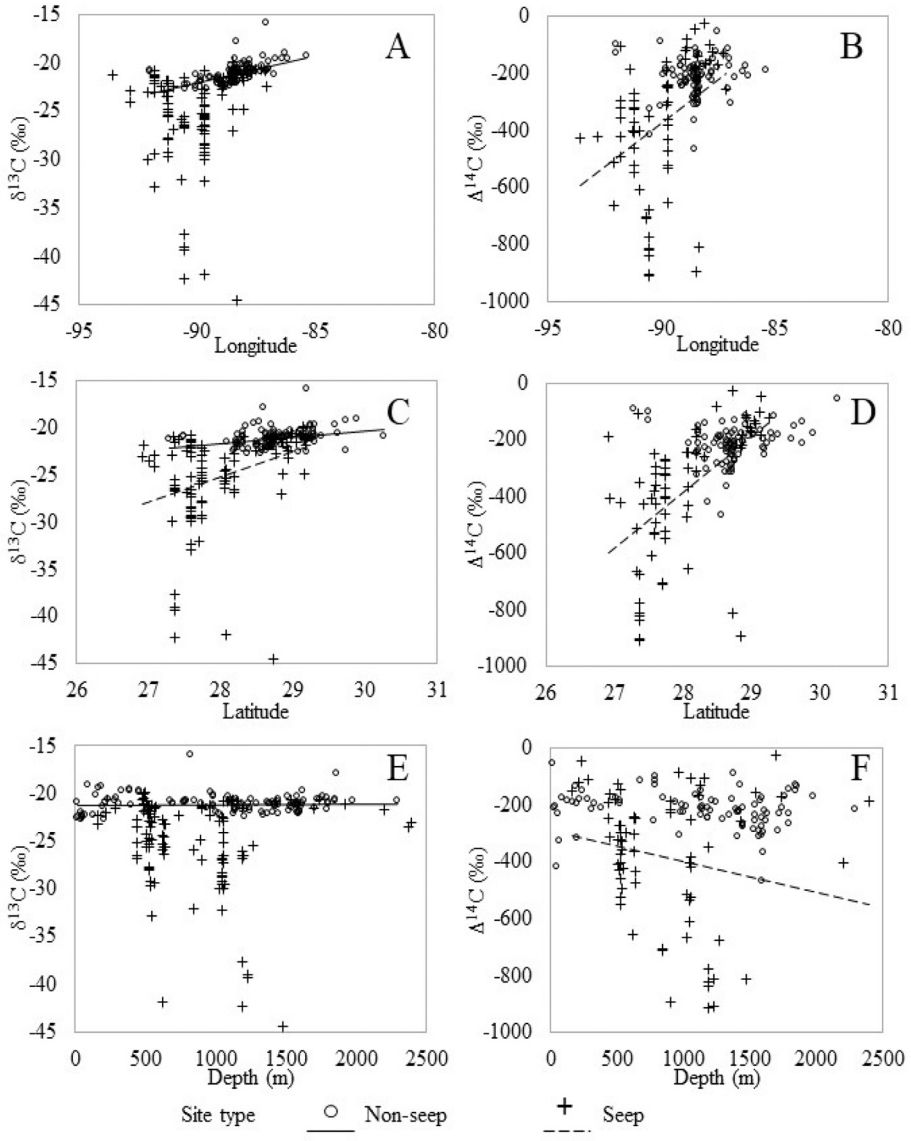

Fig. 4. Trends of isotopic data vs longitude, latitude and water depth for seep (plus sign) and non-seep (open circle) sediment: Regression lines shown for significant correlations for non-seep (solid lines) and seep only (dotted lines) (2011–2017 samples), but not all. Samples collected west of 96W (323–325, Supplementary Fig. 1), are not included in these analyses because they are isolated from the location of the main data field.

endmember and the background sediment is not great. However, mixing between riverine and primary production would lower the $\delta^{13}C$ near the mouth of river. In the eastern GOM, we find less input for seepage affecting the sediments while towards the west, towards Louisiana and Texas, there was greater influence from seeps as observed in the surface isotopic signatures (Fig. 3). The finding of no correlation with ^{14}C and longitude for non-seep sites (NCG-sites, Fig. 4B) and correlation when seep sites are included indicates that the influence of seeping material is relatively localized and does not spread beyond seep sites to non-seep sites. This also indicates that our characterization of seep and non-seep sites was robust.

There were significant relationships between latitude and both $\delta^{13}C$ (Fig. 4C, $p < 0.001$) and $\Delta^{14}C$ (Fig. 4D) for seep sites only and for all sites. This was probably driven by the presence of the mega seep site GC600, which created the main hot spot of highly depleted ^{13}C and ^{14}C carbon in Fig. 3A-B to the south of Louisiana. There was no significant relationship between water depth and $\delta^{13}C$ (Fig. 4E) or $\Delta^{14}C$ (Fig. 4F, $p = 0.0898$).

3.4. Temporal trends in the spatial data

Based on radiocarbon it was estimated that 1.6 to 2.6 $\times$ 10^{10} g of oil-derived carbon were deposited over a 2.4 $\times$ 10^{10} m^2 deep-water region surrounding the spill site (Chanton et al., 2015). This quantity represented between 0.5 and 9.1% of the released petrocarbon (5.3 $\times$ 10^{11} g carbon) with a best estimate of 3.0–4.9%. In the oil spill budget, some 11–30% of the released material was unaccounted for or listed as "other" (Lehr et al., 2010). Presumably the difference between the Chanton et al. (2015) estimate, and the quantity of missing oil could have been petrocarbon that was partially degraded to CO_2, resuspended and advected to deeper water (Diercks et al., 2018), or deposited across a broad area that was not well sampled (Passow and Hetland, 2016; Passow and Ziervogel, 2016; Romero et al., 2017).

The second goal of this study was to test the hypothesis that we would observe recovery of carbon isotope signatures at sites that received input from the DWH blowout, returning to more enriched background isotopic values over time as petrocarbon was degraded or mobilized. We created four IDW maps for surface sediment from 2010, 2011, 2012, and 2013 onward (Fig. 5). The spatial distribution of our

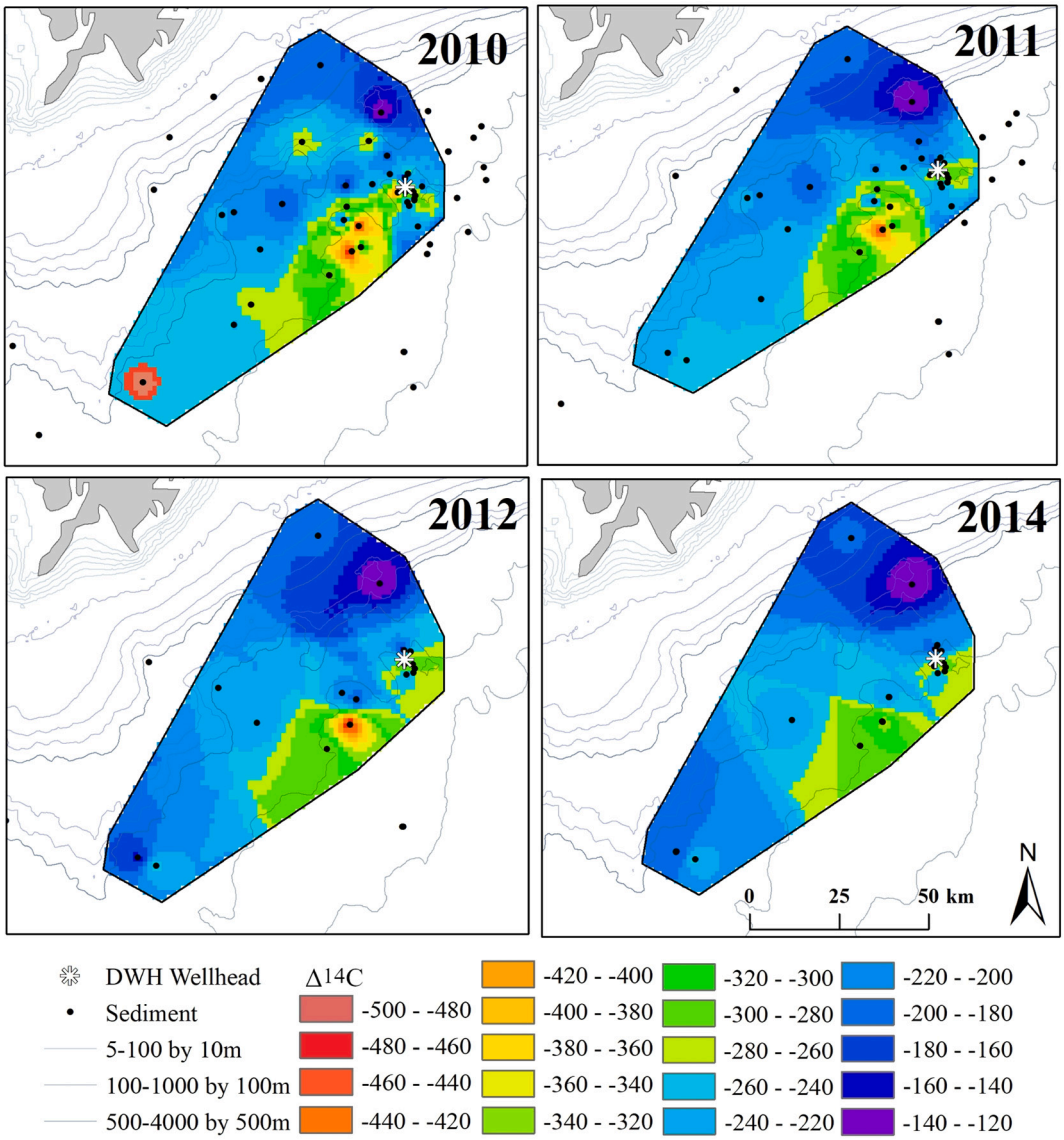

Fig. 5. Average IDW interpolations of $\Delta^{14}C$ signatures of surface sediments for 2010, 2011, 2012, and 2014 (Number of sites used in interpolation for each sample year 2013–2017: 2013: 14, 2014: 5, 2015: 8, 2016: 3, 2017: 5). Black points represent sediment core locations. The area for each 20‰ bin was calculated within the polygon. Only areas within the polygon were included in the area calculation. See Supplemental Table 1 for the points in each map.

sampling varied from year to year, and included repeated year after year sampling of many sites. In order to even out the sampling density in the maps, sites visited in later years were included in each analysis, but repeated sites sampled later than the year of the map we were making were excluded, to not dilute the signal from the analysis year. For instance, the 2010 map included all 2010 data, and data from 2011 to 2017, if those sites had not been sampled in 2010. We often found petrocarbon present in sediment collected in later years, indicating that petrocarbon would have been present there in 2010. Because of this, our map for 2010 is most likely a lower limit estimate for petrocarbon in the sediments at that time, since petrocarbon at sites from later years would have degraded more than it had in 2010, lowering the estimated petrocarbon for 2010. The 2011 map included data from 2011 to 2017; however, data from sites that were resampled in later years were not included. The 2012 map had data from 2012 to 2017, again removing repeated sampling at same sites in later years. The final map, 2014, included data from 2013 to 2017. The sampling density was too low for these four years to have individual year interpolations. The petrocarbon estimation for the final map is a best estimate for 2014. For the 2014 map, we calculated the weighted average year based on the number of samples collected over the four years. Of the 35 samples collected during these 4 years, 40% were from 2013, 14% from 2014, 23% from 2015, 9% from 2016 and 15% from 2017.

To calculate the area of petrocarbon-affected sediments, we initially used the larger polygon from Chanton et al. (2015). However, due to the lower sample size and spatial distribution from 2013 to 2017, we used a new smaller polygon, covering an area of $5x10^9 m^2$, with a 10 km boundary around the sediment collected. The new smaller polygon was concentrated in the area where we had the highest density of samples and which still captured the bulk of the affected sediments near the wellhead. Here we report the time series results of the small polygon.

The 2010 map (Fig. 5) shows a highly depleted region to the southwest of the wellhead near the border of the polygon and brighter green contours closer to the wellhead, still in the southwest direction, indicating petrocarbon deposition. The total area of highly depleted sediment, $\Delta^{14}C < -480‰$, decreased from $5.2x10^7 m^2$ in 2010 to 0 m^2 in 2011 (Table 1), indicated in the maps by the disappearance of the brightest hot spot, and the diminished intensity of the other areas of depleted radiocarbon. The sediment continued to lose the more depleted C over time, but some was still present in 2013–2017 (Fig. 5, Table 1), as

Table 1
Area and estimated mass of petrocarbon (g) within each radiocarbon $\Delta^{14}C$ contour.

$\Delta^{14}C$		Fraction petrocarbon	2010	2011	2012	2013–2017
			Area (m^2)	Area (m^2)	Area (m^2)	Area (m^2)
	≤−501	0.376	1.1×10^7	0	0	0
−500	−480	0.362	4.1×10^7	0	0	0
−480	−460	0.337	9.6×10^6	1.7×10^6	4.0×10^6	0
−460	−440	0.312	1.3×10^7	4.8×10^6	7.8×10^6	0
−440	−420	0.287	1.4×10^7	7.7×10^6	8.3×10^6	0
−420	−400	0.262	2.2×10^7	1.2×10^7	1.1×10^7	0
−400	−380	0.237	3.2×10^7	1.8×10^7	1.5×10^7	0
−380	−360	0.212	5.7×10^7	4.3×10^7	2.2×10^7	0
−360	−340	0.187	9.4×10^7	9.4×10^7	4.0×10^7	0
−340	−320	0.162	1.2×10^8	1.2×10^8	7.9×10^7	7.5×10^5
−320	−300	0.137	1.7×10^8	2.2×10^8	2.0×10^8	1.5×10^7
−300	−280	0.112	2.1×10^8	2.8×10^8	3.8×10^8	9.0×10^7
−280	−260	0.087	3.7×10^8	2.5×10^8	3.9×10^8	2.9×10^8
−260	−240	0.062	1.3×10^9	7.9×10^8	5.5×10^8	4.0×10^8
−240	−220	0.037	8.8×10^8	1.3×10^9	1.2×10^8	4.6×10^8
−220	−200	0.012	8.2×10^8	7.8×10^8	9.4×10^8	1.0×10^9
−200	−180	0	5.9×10^8	6.2×10^8	5.9×10^8	8.0×10^8
−180	−160	0	1.7×10^8	3.0×10^8	3.7×10^8	7.3×10^8
−160	−140	0	6.8×10^7	1.2×10^8	1.5×10^8	4.0×10^8
−140	−120	0	3.2×10^7	9.1×10^7	1.4×10^8	1.7×10^8
−120	−100	0	3.6×10^6	9.4×10^6	1.7×10^7	1.1×10^8
−100	−80	0	0	0	0	1.1×10^7
−80	−60	0	0	0	0	0
−60	−40	0	0	0	0	0
Total area (m^2)			4.21×10^9	3.95×10^9	3.82×10^9	2.27×10^9
% area > −200‰			17%	22%	25%	32%
g petrocarbon			1.2×10^{10}	9.5×10^9	8.8×10^9	6.0×10^9
Min estimate g petrocarbon			8.5×10^9	4.5×10^9	2.9×10^9	1.9×10^9
Max estimate g petrocarbon			2.0×10^{10}	1.5×10^{10}	1.8×10^{10}	1.2×10^{10}

not all the sediment had returned to background $\Delta^{14}C = -200‰ \pm 29‰$, but was more enriched than $\Delta^{14}C = -360‰$ (Table 1).

The total mass of petrocarbon within the small polygon decreased by 50% from $1.2x10^{10}$g in 2010 to $6.0x10^9$g in 2014 (Table 1). Uncertainties in these estimates are presented in Table 1 and Fig. 6. By 2014, we observed a decrease of 44% of the small polygon area that was ^{14}C depleted relative to the background. Our mass of petrocarbon estimates for the smaller polygon in 2010 ranged from 1.8% to 3.3% of the total released oil, decreasing to 0.4% to 2.0% by 2014. These estimates of total oil-residue deposition are low and consistent with the assertions of Passow and Ziervogel (2016) who noted the importance of the areal extent for estimating the deposition of petrocarbon by MOSSFA events. Our goal in this work was to estimate change in petrocarbon over time,

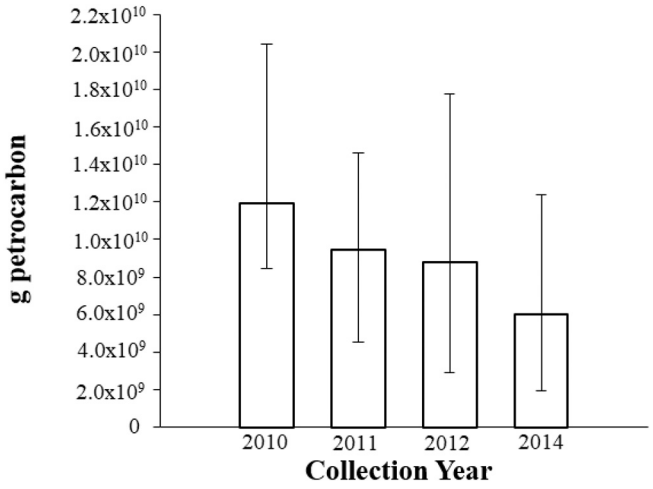

Fig. 6. Estimated g of petrocarbon in surface sediment within polygon for 2010, 2011, 2012 and 2014. Error bars indicate upper and lower limit of estimated g of petrocarbon for each year. Regression for average estimated g of petrocarbon for each year: $y = -2 \times 10^9$ (±standard deviation: 1×10^9) $x + 1 \times 10^{10}$; $r = 0.978$; $n = 4$; $p = 0.0039$.

not the total amount of petrocarbon deposition. From our estimations of the grams of petrocarbon in the polygon, there was a decrease of 2×10^9 g of petrocarbon per year over the period, presumably from a combination of in-situ biodegradation/remineralization and resuspension/mobilization (Fig. 6).

Stout et al. (2016) and Bagby et al. (2016) also found decreases in concentration and coverage area of petrocarbon compounds by 2014, including hopane. Bagby et al. (2016) found that four years after the spill, residual hopane concentrations were dependent upon overall contamination levels and that they increased across low, moderate, and high contamination levels, with 39%, 64%, and 95% of the hopane remaining. Bagby et al. (2016)'s remaining hopane estimates after four years are significantly higher than those calculated by Stout et al. (2016), who estimated 10–20% of hopane from the DWH remained after four years. Stout et al. (2016) found that the area of coverage of TPAHs in 2010 was greater than the total extent of the area of hopane, but by 2014 this observation had reversed, with greater area covered by hopane than TPAH. This was primarily due to the lower degradability of hopane compared to TPAH, but both areas were reduced when compared to the 2010 coverage.

Our estimated rate of petrocarbon loss was $-2 \times 10^9 \pm 1 \times 10^9$ g/yr or $\sim 5.5 \times 10^6 \pm 3.9 \times 10^6$ g C d^{-1} lost in the small polygon (Fig. 6). This rate is 2 ± 1.6% to 11 ± 7.8% of the estimates of hydrocarbon degradation in surface oil slicks in 2010, which ranged from 6×10^8 to 3×10^9 moles C d^{-1}, or 5×10^7 to 2.5×10^8g C d^{-1} (Edwards et al., 2011). Bagby et al. (2016) noted that oil degradation rates were slower once material was deposited in the sediment relative to rates occurring while the material was suspended in the water column, and that the contamination level also affected the degradation rate. Our subject polygon was focused on the most impacted area, so following Bagby et al. (2016) conclusions, this area would have had a slower degradation rate than less impacted areas. And as discussed above, radiocarbon reflects petrocarbon, transformed petroleum material following biodegradation, weathering, oxygenation or loss of lighter components including methane or oil derived carbon assimilated or incorporated into microbial biomass, which would remain in the sediments. So, for the sake of illustration, if a hopane molecule was transformed and incorporated into microbial biomass, we would still observe that residue, while Stout et al. (2016) and Bagby et al. (2016) would not. Hopane and other crude oil markers quickly form oxygenated compounds that are not identified as the original biomarker anymore (Aeppli et al., 2012). This transformation is seen as a decrease in the hopane residue, but the remaining

oxygenated compound could be even more toxic than the original oil material. Thus, our radiocarbon-derived degradation rates are likely on the lower end of estimates determined by other means, unless the loss of petrocarbon on the seafloor is driven by resuspension and mobilization (Diercks et al., 2018), in which case they should be similar. Our results indicate that while recovery is proceeding on the seafloor of the Gulf, petrocarbon residues continue to persist over the time scale of this study. The residual hydrocarbons present likely influence our estimates of isotopic baseline towards more depleted values.

Funding information

This research was made possible by grants from The Gulf of Mexico Research Initiative through its consortiums: Ecosystem Impacts of Oil & Gas Inputs to the Gulf (ECOGIG), The Center for the Integrated Modeling and Analysis of the Gulf Ecosystem (C-Image), Deep Sea to Coast Connectivity in the Eastern Gulf of Mexico (Deep-C) and the REDIRECT project funded by the Gulf of Mexico Research Initiative via the University of Southern Mississippi and its partners. This is ECOGIG Contribution # 516.

CRediT authorship contribution statement

Kelsey L. Rogers: Investigation, Visualization, Writing – original draft. **Samantha H. Bosman:** Writing – review & editing. **Natalie Wildermann:** Visualization. **Brad E. Rosenheim:** Investigation, Formal analysis. **Joseph P. Montoya:** Investigation, Project administration. **David Hollander:** Funding acquisition, Investigation. **Tingting Zhao:** Formal analysis. **Jeffrey P. Chanton:** Conceptualization, Resources, Writing – original draft, Writing – review & editing, Supervision.

Declaration of competing interest

The authors declare that they have no known competing financial interests or personal relationships that could have appeared to influence the work reported in this paper.

Acknowledgements

AMS samples were run at the University of Georgia Center for Applied Isotopic Studies, and the National Oceanographic Center for Accelerator Mass Spectrometry at Woods Hole Oceanographic. We thank Alexander Cherinsky, Ann McNichol, Kathryn Elder, and Mark Roberts. Samples were collected from the RV *Endeavor*, RV *Pelican* and the RV *Weatherbird* and we thank their crews, and Ryan Sibert, and Andy Montgomery of UGA. We thank Burt Wolff and Yang Wang for use of the facilities at the National High Magnetic Field Laboratory. Some sample preparation and analyses were performed in the Stable Isotope Lab within the Geochemistry Program at the National High Magnetic Field Laboratory, which is supported by National Science Foundation Cooperative Agreement No. DMR-1644779 and the State of Florida.

Data accessibility statement

Data deposition: data are publicly available through the Gulf of Mexico Research Initiative Information & Data Cooperative (GRIIDC) at https://data.gulfresearchinitiative.org, DOI https://doi.org/10.7266/N7Q52N7D.

Appendix A. Supplementary data

Supplementary data to this article can be found online at https://doi.org/10.1016/j.marpolbul.2021.112076.

References

Adhikari, P.L., Maiti, K., Overton, E.B., Rosenheim, B.E., Marx, B.D., 2016. Distributions and accumulation rates of polycyclic aromatic hydrocarbons in the northern Gulf of Mexico sediments. Environ. Pollut. 212, 413–423. https://doi.org/10.1016/j.envpol.2016.01.064.

Aeppli, C., Carmichael, C.A., Nelson, R.K., Lemkau, K.L., Graham, W.M., Redmond, M.C., Valentine, D.L., Reddy, C.M., 2012. Oil weathering after the Deepwater Horizon disaster led to the formation of oxygenated residues. Environ. Sci. Technol. 46, 8799–8807. https://doi.org/10.1021/es3015138.

Aeppli, C., Swarthout, R.F., O'Neil, G.W., Katz, S.D., Nabi, D., Ward, C.P., Nelson, R.K., Sharpless, C.M., Reddy, C.M., 2018. How persistent and bioavailable are oxygenated Deepwater Horizon oil transformation products? Environ. Sci. Technol. 52 (13), 7250–7258. https://doi.org/10.1021/acs.est.8b01001.

Bagby, S.C., Reddy, C.M., Aeppli, C., Fisher, G.B., Valentine, D.L., 2016. Persistence and biodegradation of oil at the ocean floor following Deepwater Horizon. Proc. Natl. Acad. Sci. https://doi.org/10.1073/pnas.1610110114.

Bianchi, T.S., Mitra, S., McKee, B.A., 2002. Sources of terrestrially-derived organic carbon in lower Mississippi River and Louisiana Shelf sediments: implications for differential sedimentation and transport at the coastal margin. Mar. Chem. 77 (2–3), 211–223. https://doi.org/10.1016/S0304-4203(01)00088-3.

Bosman, S.H., Chanton, J.P., Rogers, K.L., 2017. Using Stable and Radiocarbon Analyses as a Forensic Tool to Find Evidence of Oil in the Particulates of the Water Column and on the Seafloor Following the 2010 Gulf of Mexico Oil Spill. Elsevier Inc. https://doi.org/10.1016/B978-0-12-804434-6.00029-X

Bostic, J.T., Aeppli, C., Swarthout, R.F., Reddy, C.M., Ziolkowski, L.A., 2018. Ongoing biodegradation of Deepwater Horizon oil in beach sands: insights from tracing petroleum carbon into microbial biomass. Mar. Pollut. Bull. 2018 (126), 130–136. https://doi.org/10.1016/j.marpolbul.2017.10.058.

Brooks, G.R., Larson, R.A., Schwing, P.T., Romero, I., Moore, C., Reichart, G.J., Jilbert, T., Chanton, J.P., Hastings, D.W., Overholt, W.a., et al., 2015. Sedimentation pulse in the NE Gulf of Mexico following the 2010 DWH blowout. PLoS One 10 (7), 1–24. https://doi.org/10.1371/journal.pone.0132341.

Burd, A.B., Chanton, J.P., Daly, K.L., Gilbert, S., Passow, U., Quigg, A., 2020. The science behind marine-oil snow and MOSSFA: past, present, and future. Prog. Oceanogr. 187, 102398. https://doi.org/10.1016/j.pocean.2020.102398.

Cai, Y., Guo, L., Wang, X., Aiken, G., 2015. Abundance, stable isotopic composition, and export fluxes of DOC, POC, and DIC from the Lower Mississippi River during 2006-2008. J. Geophys. Res. Biogeosci. 120, 2273–2288. https://doi.org/10.1002/2015JG003139.

Chanton, J.P., Cherrier, J., Wilson, R.M., Sarkodee-Adoo, J., Bosman, S., Mickle, A., Graham, W.M., 2012. Radiocarbon evidence that carbon from the Deepwater Horizon spill entered the planktonic food web of the Gulf of Mexico. Environ. Res. Lett. 7 (4), 045303 https://doi.org/10.1088/1748-9326/7/4/045303.

Chanton, J., Zhao, T., Rosenheim, B.E., Joye, S., Bosman, S., Brunner, C., Yeager, K.M., Diercks, A.R., Hollander, D., 2015. Using natural abundance radiocarbon to trace the flux of petrocarbon to the seafloor following the Deepwater Horizon oil spill. Environ. Sci. Technol. 49 (2), 847–854. https://doi.org/10.1021/es5046524.

Chanton, J. P.; Giering, S. L. C.; Bosman, S. H.; Rogers, K. L.; Sweet, J.; Asper, V. L.; Diercks, A. R.; Passow, U. Isotopic composition of sinking particles: oil effects, recovery and baselines in the Gulf of Mexico. Elem. Sci. Anth. 2018, 6 (43), DOI: https://doi.org/10.1525/elementa.298.

Cherrier, J., Sarkodee-Adoo, J., Guilderson, T.P., Chanton, J.P., 2014. Fossil carbon in particulate organic matter in the Gulf of Mexico following the Deepwater Horizon event. Environ. Sci. Technol. Lett. 1 (1), 108–112. https://doi.org/10.1021/ez400149c.

Choi, Y., Wang, Y., 2004. Dynamics of carbon sequestration in a coastal wetland using radiocarbon measurements. Global Biogeochem. Cy. 18 (4), 1–12. https://doi.org/10.1029/2004GB002261.

Corbett, D.R., McKee, B., Duncan, D., 2004. An evaluation of mobile mud dynamics in the Mississippi River deltaic region. Mar. Geol. 209 (1–4), 91–112. https://doi.org/10.1016/j.margeo.2004.05.028.

Corbett, D.R., McKee, B., Allison, M., 2006. Nature of decadal-scale sediment accumulation on the western shelf of the Mississippi River delta. Cont. Shelf Res. 26 (17–18), 2125–2140. https://doi.org/10.1016/j.csr.2006.07.012.

Crespo-Medina, M., Meile, C.D., Hunter, K.S., Diercks, A., Asper, V., Orphan, V.J., Tavormina, P.L., Nigro, L.M., Battles, J.J., Chanton, J.P., Shiller, A.M., Joung, D.-J., Amon, R.M.W., Bracco, A., Montoya, J.P., Villareal, T.A., Wood, A.M., Joye, S.B., 2014. The rise and fall of methanotrophy following a deepwater oil-well blowout. Nat. Geosci. 7, 423–427. https://doi.org/10.1038/NGEO2156.

Daly, K.L., Passow, U., Chanton, J., Hollander, D., 2016. Assessing the impacts of oil-associated marine snow formation and sedimentation during and after the Deepwater Horizon oil spill. Anthropocene 13, 18–33. https://doi.org/10.1016/j.ancene.2016.01.006.

De La Rocha, C.L., Passow, U., 2007. Factors influencing the sinking of POC and the efficiency of the biological carbon pump. Deep. Res. Part II Top. Stud. Oceanogr. 54, 639–658. https://doi.org/10.1016/j.dsr2.2007.01.004.

Diercks, A., Dike, C., Asper, V.L., Dimarco, S.F., Jeffrey, P., 2018. Scales of seafloor sediment resuspension in the northern Gulf of Mexico. Elem. Sci. Anth. 6 (1), 32. https://doi.org/10.1525/elementa.285.

D'souza, N.A., Subramaniam, A., Juhl, A.R., Hafez, M., Chekalyuk, A., Phan, S., Yan, B., MacDonald, I.R., Weber, S.C., Montoya, J.P., 2016. Elevated surface chlorophyll associated with natural oil seeps in the Gulf of Mexico. Nat. Geosci. 9 (January), 1–4. https://doi.org/10.1038/ngeo2631.

Edwards, B. R.; Reddy, C. M.; Camilli, R.; Carmichael, C. A.; Longnecker, K.; Van Mooy, B. A S. Rapid microbial respiration of oil from the Deepwater Horizon spill in

offshore surface waters of the Gulf of Mexico. Environ. Res. Lett. 2011, 6 (3), 035301. doi:https://doi.org/10.1088/1748-9326/6/3/035301.
Giering, S.L.C., Yan, B., Sweet, J., Asper, V., Diercks, A., Chanton, J.P., Pitiranggon, M., 2018. The ecosystem baseline for particle flux in the northern Gulf of Mexico. Elem. Sci. Anth. 6, 6. https://doi.org/10.1525/elmenta.264.
Goni, M.A., Ruttenberg, K.C., Eglinton, T.I., 1998. A reassessment of the sources and importance of land-derived organic matter in surface sediments from the Gulf of Mexico. Geochim. Cosmochim. Acta 62 (18), 3055–3075. https://doi.org/10.1016/S0016-7037(98)00217-8.
Gordon, E.S., Goni, M.A., 2003. Sources and distribution of terrigenous organic matter delivered by the Atchafalaya River to sediments in the northern Gulf of Mexico. Geochim. Cosmochim. Acta 67 (13), 2359–2375. https://doi.org/10.1016/S0016-7037(02)01412-6.
Graham, W.M., Condon, R.H., Carmichael, R.H., D'Ambra, I., Patterson, H.K., Linn, L.J., Hernandez Jr., F.J., 2010. Oil carbon entered the coastal planktonic food web during the Deepwater Horizon oil spill. Environ. Res. Lett. 5 (4), 045301 https://doi.org/10.1088/1748-9326/5/4/045301.
Lehr, W., Bristol, S., Possolo, A., 2010. Federal Interagency Solutions Group, Oil Budget Calculator Science and Engineering Team. Oil Budget Calculator, Technical Documentation. Tech. Doc. https://www.restorethegulf.gov/sites/default/files/documents/pdf/OilBudgetCalc_Full_HQ-Print_111110.pdf.
MacDonald, I.R., Garcia-Pineda, O., Beet, A., Daneshgar Asl, S., Feng, L., Graettinger, G., French-Mccay, D., Holmes, J., Hu, C., Huffer, F., et al., 2015. Natural and unnatural oil slicks in the Gulf of Mexico. J. Geophys. Res. Ocean. 120 (12), 8364–8380. https://doi.org/10.1002/2015JC011062.
Mason, O.U., Scott, N.M., Gonzalez, A., Robbins-Pianka, A., Bælum, J., Kimbrel, J., Bouskill, N.J., Prestat, E., Borglin, S., Joyner, D.C., et al., 2014. Metagenomics reveals sediment microbial community response to Deepwater Horizon oil spill. ISME J. 8 (7), 1464–1475. https://doi.org/10.1038/ismej.2013.254.
Passow, U., Hetland, R.D., 2016. What happened to all of the oil? Oceanography 29 (3), 88–95. https://doi.org/10.5670/oceanog.2016.73.
Passow, U., Ziervogel, K., 2016. Marine snow sedimented oil released during the Deepwater Horizon spill. Oceanography 29 (3), 118–125. https://doi.org/10.5670/oceanog.2016.76.
Passow, U., Ziervogel, K., Asper, V., Diercks, A., 2012. Marine snow formation in the aftermath of the Deepwater Horizon oil spill in the Gulf of Mexico. Environ. Res. Lett. 7 (3), 035301 https://doi.org/10.1088/1748-9326/7/3/035301.
Rogers, K.L., Bosman, S.H., Lardie-Gaylord, M., McNichol, A., Rosenheim, B.E., Montoya, J.P., Chanton, J.P., 2019a. Petrocarbon evolution: ramped pyrolysis/oxidation and isotopic studies of contaminated oil sediments from the Deepwater Horizon oil spill in the Gulf of Mexico. PLoS One 14 (2), e0212433. https://doi.org/10.1371/journal.pone.0212433.
Rogers, K.L.; Bosman, S. H., Weber, S., Magen C., Montoya, J. P., and Chanton, J. P. Sources of carbon to suspended particulate organic matter in the northern Gulf of Mexico. Elem. Sci. Anth. 2019b, 7(51). doi:https://doi.org/10.1525/elementa.389.
Romero, I.C., Toro-Farmer, G., Diercks, A.R., Schwing, P., Muller-Karger, F., Murawski, S., Hollander, D.J., 2017. Large-scale deposition of weathered oil in the Gulf of Mexico following a deep-water oil spill. Environ. Poll. 228, 179–189. https://doi.org/10.1016/j.envpol.2017.05.019.
Rosenheim, B.E., Pendergraft, M.A., Flowers, G.C., Carney, R., Sericano, J.L., Amer, R.M., Chanton, J., Dincer, Z., Wade, T.L., 2016. Employing extant stable carbon isotope data in Gulf of Mexico sedimentary organic matter for oil spill studies. Deep. Res. Part II Top. Stud. Oceanogr. 129, 249–258. https://doi.org/10.1016/j.dsr2.2014.03.020.
Ruddy, B.M., Huettel, M., Kostka, J.E., Lobodin, V.V., Bythell, B.J., McKenna, A.M., Aeppli, C., Reddy, C.M., Nelson, R.K., Marshall, A.G., et al., 2014. Targeted petroleomics: analytical investigation of Macondo Well oil oxidation products from Pensacola Beach. Energy Fuel 28 (6), 4043–4050. https://doi.org/10.1021/ef500427n.
Ryerson, T.B., Camilli, R., Kessler, J.D., Kujawinski, E.B., Reddy, C.M., Valentine, D.L., Atlas, E., Blake, D.R., de Gouw, J., Meinardi, S., et al., 2012. Chemical data quantify Deepwater Horizon hydrocarbon flow rate and environmental distribution. Proc. Natl. Acad. Sci. 109 (50), 20246–20253. https://doi.org/10.1073/pnas.1110564109.
Schwing, P.T., Brooks, G.R., Larson, R.A., Holmes, C.W., O'Malley, B.J., Hollander, D.J., 2017. Constraining the spatial extent of marine oil snow sedimentation and flocculent accumulation following the Deepwater Horizon event using an excess 210Pb flux approach. Environ. Sci. Technol. 51 (11), 5962–5968. https://doi.org/10.1021/acs.est.7b00450.
Stout, S.A., Rouhani, S., Liu, B., Oehrig, J., Ricker, R.W., Baker, G., Lewis, C., 2016. Assessing the footprint and volume of oil deposited in deep-sea sediments following the Deepwater Horizon oil spill. Mar. Pollut. Bull. https://doi.org/10.1016/j.marpolbul.2016.09.046.
Stuiver, M., Polach, H.A., 1977. Discussion: reporting of 14C data. Radiocarbon 19 (3), 355–363.
Sun, Y., Chen, Z., Xu, S., Cai, P., 2005. Stable carbon and hydrogen isotopic fractionation of individual n-alkanes accompanying biodegradation: evidence from a group of progressively biodegraded oils. Org. Geochem. 36 (2), 225–238. https://doi.org/10.1016/j.orggeochem.2004.09.002.
Valentine, D.L., Kessler, J.D., Redmond, M.C., Mendes, S.D., Heintz, M.B., Farwell, C., Hu, L., Kinnaman, F.S., Yvon-Lewis, S., Du, M., et al., 2010. Propane respiration jump-starts microbial response to a deep oil spill. Science 330 (6001), 208–211. https://doi.org/10.1126/science.1196830.
Valentine, D.L., Fisher, G.B., Bagby, S.C., Nelson, R.K., Reddy, C.M., Sylva, S.P., Woo, M. A., 2014. Fallout plume of submerged oil from Deepwater Horizon. Proc. Natl. Acad. Sci. 111 (45), 15906–15911. https://doi.org/10.1073/pnas.1414873111.
White, H.K., Reddy, C.M., Eglinton, T.I., 2008. Radiocarbon-based assessment of fossil fuel-derived contaminant associations in dediments. Environ. Sci. Technol. 42, 5428–5434. https://doi.org/10.1021/es800478x.
Wilson, R.M., Hopple, A., Tfaily, M.M., Sebestyen, S.D., Schadt, C.W., Pfeifer-Meister, L., Medvedeff, C., McFarlane, K.J., Kostka, J.E., Kolton, M., et al., 2016. Stability of peatland carbon to rising temperatures. Nat. Commun. 7, 13723. https://doi.org/10.1038/ncomms13723.
Yan, B., Passow, U., Chanton, J.P., Nöthig, E.-M., Asper, V., Sweet, J., Pitiranggon, M., Diercks, A., Pak, D., 2016. Sustained deposition of contaminants from the Deepwater Horizon spill. Proc. Natl. Acad. Sci., 201513156 https://doi.org/10.1073/pnas.1513156113.
Zafiriou, O.C., 1973. Petroleum hydrocarbons in Narragansett Bay. Estuar. Coast. Mar. Sci. 1973 (1), 81–87. https://doi.org/10.1016/0302-3524(73)90060-1.